Amplitude modulation and surface wave generation in a complex plasma monolayer

Srimanta Maity [1,*] and Garima Arora [2,†]

[1]*ELI Beamlines Facility, The Extreme Light Infrastructure ERIC, Za Radnicí 835, 25241 Dolní Břežany, Czech Republic*
[2]*Institute of Plasma Physics of the Czech Academy of Sciences, 18200 Prague, Czech Republic*

The response of a two-dimensional plasma crystal to an externally imposed initial perturbation has been explored using molecular dynamics (MD) simulations. A two-dimensional (2D) monolayer of micron-sized charged particles (dust) is formed in the plasma environment under certain conditions. The particles interacting via Yukawa pair potential are confined in the vertical ($\hat{z}$) direction by an external parabolic confinement potential, which mimics the combined effect of gravity and the sheath electric field typically present in laboratory dusty plasma experiments. An external perturbation is introduced in the medium by displacing a small central region of particles in the vertical direction. The displaced particles start to oscillate in the vertical direction, and their dynamics get modulated through a parametric decay process generating beats. It has also been shown that the same motion is excited in the dynamics of unperturbed particles. A simple theoretical model is provided to understand the origin of the beat motions of particles. Additionally, in our simulations, concentric circular wavefronts propagating radially outward are observed on the surface of the monolayer. The physical mechanism and parametric dependence of the observed phenomena are discussed in detail. This research sheds light on the medium's ability to exhibit macroscopic softness, a pivotal characteristic of soft matter, while sustaining surface wave modes. Our findings are also relevant to other strongly coupled systems, such as colloids and classical one-component plasmas.

I. INTRODUCTION

Complex plasma has been proven to be a remarkable medium to study waves [1,2], crystallization [3–6], phase transition [7–9], cluster formation [10–12], crystal cracking [13], lane formation [14], flow-induced excitations [15–18], and many more. A low-power laser and standard camera are sufficient to visualize, perturb, and capture the dynamics of the medium due to its response with unique length (of the order of millimeters) and timescales (of the order of milliseconds). Complex plasma is a system of micron or submicron-sized dust particles suspended in the plasma environment. The suspended dust particles acquire large amounts of charge, which leads to much higher Coulomb potential energy with respect to the average thermal energy of particles. The medium exhibits from a fluid to a crystalline phase depending upon the ratio between Coulomb potential energy and dust thermal energy. Complex plasma is also considered a new state of soft matter where the medium's equilibrium properties and dynamical response depend upon the external conditions [19].

Complex plasma medium has been shown to sustain various waves, e.g., linear waves such as dust acoustic waves (DAW) [1], transverse shear waves [20], and nonlinear waves such as solitons [16,18,21] and shocks [22]. Various nonlinear structures [23], e.g., voids [24], Mach cones [25], vortex [26],

etc., have also been reported in a dusty plasma medium. The first DAW was theoretically predicted by Rao *et al.* [27] and experimentally realized by Barkan *et al.* [28] in liquid and gaseous states. Kaw and Sen [20] predicted the new mode called transverse shear wave using a generalized hydrodynamic (GHD) model in dusty plasma when the medium is in a strongly coupled fluid state. Pramanik *et al.* [29] confirmed this transverse shear wave experimentally in three-dimensional strongly coupled dusty plasma fluid.

The research on dust lattice waves has also been running alongside [30] since the discovery of plasma crystals. Typically, dust lattice waves are excited in the laboratory by applying a modulating voltage to the wire near the dust crystal [31]. Another novel technique introduced to excite lattice waves is using the radiation pressure of a laser, which does not perturb the plasma environment and is considered far better than the modulated voltage technique. Nunomoura *et al.* [32] used the same method to excite the in-plane transverse shear wave in monolayer dusty plasma crystal. The vertical vibrations of dust grains in sheath region also induce low-frequency modes and are first studied theoretically by Vladimirov *et al.* [33] in the 1D chain. They obtained the dispersion relation of the off-plane motions of the particles using the fluctuation spectra obtained from the thermal motion of the particles and found that it follows inverse-optic dispersion characteristics. The theory in the 1D Yukawa chain is experimentally verified by Liu *et al.* [34]. The knowledge of unique dispersion characteristics is extended to 2D crystals and same characteristics are verified in theory [35–37], simulations [38], and experiments [39–42]. Samsonov *et al.* [39]

———————
*srimantamaity96@gmail.com
†garimaarora@gmail.com

tried to find the transverse off-plane dispersion relation experimentally by applying a negative pulse to the wire placed beneath the 2D monolayer. They used wire excitation in which they had no control over the excitation frequency and wave number. Amplitude modulation of dust lattice waves (DLW) was numerically studied by Melandso [30]. A theoretical model for the slow modulation of the DLW was reported by Amin *et al.* [43] by introducing a fast and slow motion of dust plasma as an initial condition. There are also reports on the large amplitude oscillations in the vertical direction, which leads to instability and phase transition [9,44].

In the present work, we have investigated the vertical dynamics of particles in an externally perturbed crystalline monolayer using Molecular Dynamics (MD) simulations. This study is mainly devoted to the characteristics response and its parametric dependence of a 2D plasma crystal to an externally imposed perturbation. Unlike the previous studies, we introduced the external perturbation only within a small region of a large crystalline structure. The motivation of our work is to capture the process of the energy transport mechanism from the initially perturbed region to the undisturbed region of the monolayer. In particular, we investigate how the initially disturbed particles respond to external perturbation, how this information spreads to the region far away from the initially perturbed area, and what processes govern the dynamics of particles. The external perturbation is introduced by displacing the small region of particles at the center of the monolayer in the downward $(-\hat{z})$ direction. This method can be easily realized in the laboratory, e.g., by focusing a laser pulse perpendicular to the plane of a complex plasma monolayer. Recently, in our previous work [9], we used a similar technique and showed a first-order phase transition in the 2D dust crystal induced by parametric decay instability above a threshold value of initial displacement. In the present work, we introduce a small initial displacement to the particles so that the medium remains in the crystalline state. We have studied the dynamics of the perturbed as well as unperturbed particles by tracking the single-particle trajectories. It has been found that the amplitude of initially displaced particles modulates via a parametric decay process and generates beats motion. A similar motion is also observed in the dynamics of unperturbed particles. The parametric decay process has been observed in many other aspects of plasma physics, inertial [45] and magnetic confinement fusion [46], and laser-plasma interactions [47]. In our study, we have identified the dependence of the parametric decay process on different system parameters, such as confinement potential, perturbation radius, dust density in the 2D monolayer, and dust-neutral collision frequency. We have also observed that the beat motion of the particles initiates a collective response generating circular transverse wavefronts called surface waves, which propagate radially outwards from the center of the monolayer. The atomistic picture of the wave reveals a mixture of longitudinal and transverse motion of particles similar to the surface wave in different media. The dispersion analysis of the surface wave has also been carried out and found that it follows the same dispersion characteristics as the theoretically predicted transverse shear wave. A simple theoretical model is also provided in support of our simulation results. In our simulations, we have not considered the ion motions in the

vertical direction, which may affect the dispersion properties of the surface wave modes observed in our study.

The whole paper is divided into different sections. In Sec. II, MD simulation details are described. In Sec. III A, the amplitude modulation process on the perturbed region in response to the external perturbation is discussed. The dependence of amplitude modulation phenomena on various system parameters, e.g., confinement frequency, dust density, and radius of the externally perturbed region, is described in various subsections. In Sec. III B, the effect of dust-neutral collisions on the phenomena observed in our study has been discussed. Section III C provides a theoretical model supporting our simulation observations. The collective response of the medium to the external perturbation is described in Sec. III D. At last, all the results from simulation and modeling are summarised in Sec. IV.

II. SIMULATION DETAILS

In this work, three-dimensional (3D) molecular dynamics (MD) simulations have been performed using an open-source massively parallel classical MD code LAMMPS [48]. Initially, ten thousand charged point particles (dust grains) interacting with each other via Yukawa pair potential have been distributed randomly inside a rectangular simulation box. In our simulation, we have considered periodic boundary conditions in all three directions. In our study, we have considered the charge (Q) and mass (m_d) of the dust grains to be $Q = -1000e$ and $m_d = 1.0 \times 10^{-13}$ kg, respectively. Here, e represents the magnitude of an electronic charge. In the vertical ($\hat{z}$) direction, a parabolic electrostatic potential $V_{\text{ext}} = (m_d \omega_v^2 / 2Q)(z - L_z/2)^2$ has been applied, which provides the vertical confinement of charged dust particles. Here, L_z represents the length of the simulation box along $\hat{z}$. The parameter ω_v defines the angular frequency at which the particles would oscillate in the external parabolic potential if they do not interact with each other. The equation of motion of any ith particle can be expressed as

$$m_d \frac{d^2 \mathbf{r}_i}{dt^2} = -Q \sum_{j=1}^{N-1} \nabla U(r_{i,j}) - Q \nabla V_{\text{ext}}, \qquad (1)$$

where r_i and r_j are the positions of the ith and jth particles at a particular time, respectively, and $U(r_{i,j}) = (Q/4\pi\epsilon_0 |\mathbf{r}_j - \mathbf{r}_i|) \exp(-|\mathbf{r}_j - \mathbf{r}_i|/\lambda_D)$ represents Yukawa pair potential between ith and jth particle. Here, N represents the total number of particles.

Initially, the system of charged particles has been relaxed to a thermal equilibrium state with a desired value of temperature $T = 300$ K. A Nose-Hoover thermostat [49–51] is used for this purpose. For our chosen values of system parameters, particles in thermal equilibrium form a crystalline monolayer in the x-y plane levitating at a height $z = L_z/2$. Later, the thermostat is disconnected, and the system is allowed to evolve in a microcanonical ensemble where the total number of particles (N), system volume (V), and total energy (E) remain conserved. Under this condition, we have imposed a perturbation to the medium, i.e., monolayer, by displacing a few particles over a distance d along the $-\hat{z}$ direction, as illustrated by the schematic in Fig. 1. It is to be noticed that
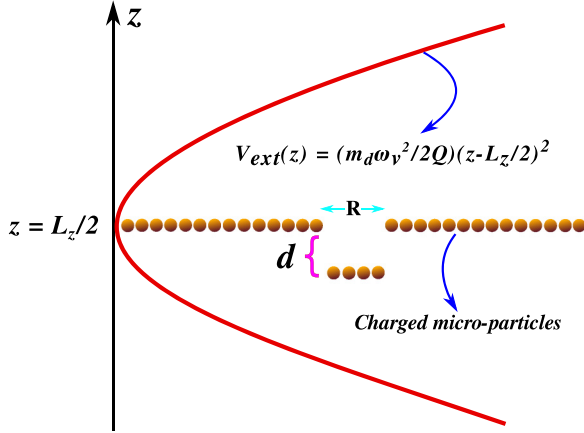
FIG. 1. The schematic of the simulation setup is shown. A parabolic potential (V_{ext}) with a minimum at the location $z = L_z/2$ is externally applied in the vertical direction ($\hat{z}$). In equilibrium, charged microparticles interacting via Yukawa pair potential form a monolayer levitating at a height $z = L_z/2$ under the effect of V_{ext}. Then, the particles located within a radius R around the center of this monolayer are displaced vertically ($-\hat{z}$ direction) by a distance d from their equilibrium positions.

only the particles which were initially located within a small circular region of radius R around the center of the monolayer have been displaced.

In our study, the plasma Debye length providing the screening in the pair interactions between particles is chosen to be $\lambda_D = 5 \times 10^{-3}$ m. We have considered the initial displacement to be $d = \lambda_D$ in all the cases. However, n_d, ω_v, and R have been varied in our simulation, which will be discussed in Sec. III. We have chosen a particular value of $n_d = n_0 = 1 \times 10^6$ m^{-2} as a reference and has been used for normalization purposes. The 2D dust plasma frequency associated with n_0 is given by $\omega_n = \sqrt{Q^2/2\pi\epsilon_0 m_d a^3} = 22.63$ s^{-1}. Here, $a = (\pi n_0)^{-1/2}$ represents the average interparticle distance in the 2D monolayer. In our study, the length and timescales are normalized by λ_D and ω_n^{-1}, respectively. The velocity of the particles is normalized by the thermal velocity $v_{th} = \sqrt{k_B T/m_d}$, where k_B represents the Boltzmann constant. The simulation time step is considered to be $dt = 0.001\omega_n^{-1}$, which is small enough to track the fastest dynamics of particles.

III. RESULTS AND DISCUSSION

Initially, randomly distributed charged microparticles interacting via screened Coulomb pair potential is allowed to relax under the influence of an externally applied parabolic potential. The final equilibrium state depends on the system parameters, i.e., dust charge Q, dust density n_d, plasma Debye length λ_D, and parabolic confinement potential characterized by ω_v. For our chosen values of simulation parameters, charged dust particles relax to an equilibrium state, forming a monolayer plasma crystal. This crystalline monolayer levitates inside the simulation box at a certain height of $z = L_z/2$, i.e., at the location of the minima of the external parabolic potential well, as illustrated by the schematic in Fig. 1. Then,

we displaced a few particles within a radius R around the center of this monolayer by a distance d along the vertical direction ($-\hat{z}$) to impose a disturbance in the medium. This has also been illustrated by the schematic in Fig. 1. We have analyzed various features of our observation as a consequence of this external perturbation in the medium and presented them in the following subsections.

A. Amplitude modulation via parametric decay process

The initially displaced particles exhibit vertical oscillatory motion around the x-y plane of the monolayer under the influence of the parabolic potential well. If the particles do not interact with each other, they will oscillate with a certain frequency determined by the restoring force associated with the external parabolic potential, i.e., ω_v. In that case, the amplitude of their oscillatory motions will also remain constant, determined by the initial displacement d. However, the dynamics of each particle are strongly coupled with each other via screened Coulomb pair potential. The pair interaction strength is determined by particle density (n_d) and plasma Debye length (λ_D). It has been observed that the amplitude of vertical oscillations does not remain constant but gets modified periodically with time. Thus, instead of oscillating with a constant frequency and amplitude, a train of pulses (beats) with different frequencies appears in the oscillatory motions of the particles. This is a clear signature of amplitude modulation of the initially induced vertical oscillatory motion. It is worth mentioning that when we displace the entire crystalline plane vertically from its equilibrium position, all the particles oscillate with constant frequency ω_v and amplitude d. Thus, the amplitude modulation observed in our study occurs due to the finite boundary (R) of the initial perturbation. To analyze these co-related dynamics in more detail, we chose a single particle initially located at the center of the monolayer and tracked its dynamics with time. In the following subsections, we have depicted the time history of the dynamics of this particle for different cases with the changing values of system parameters, e.g., confinement frequency (ω_v), dust density (n_d), and the radius of the initially perturbed region (R).

1. Dependence on confinement potential

We performed a series of simulations for changing values of ω_v with a fixed dust density $n_d = 1.0n_0$ and perturbation radius $R = 5\lambda_D$ to investigate the effect of external confinement potential on the amplitude modulation phenomena observed in our study. As stated earlier, we tracked a perturbed particle initially located at the center of the monolayer in each case. The time evolution of $\hat{z}$ component of velocity (v_z) of the tracked particle is shown in Fig. 2 for three different simulation runs with changing values of ω_v. In all three cases, v_z oscillates with time, and a train of pulses or beats appears in the time profile of v_z. It is also seen that the amplitudes of the beats are different in different cases and decay with time. Moreover, the beat frequency and the decay rate of the beat amplitude decrease as we increase the value of ω_v.

To analyze the properties of these beats, we have evaluated the Fourier spectra from the time series data of v_z and v_{zm} of the tracked particle. Here, v_{zm} represents the peak values of $v_z(t)$, and thus, the Fourier spectra of $v_{zm}(t)$ will give the
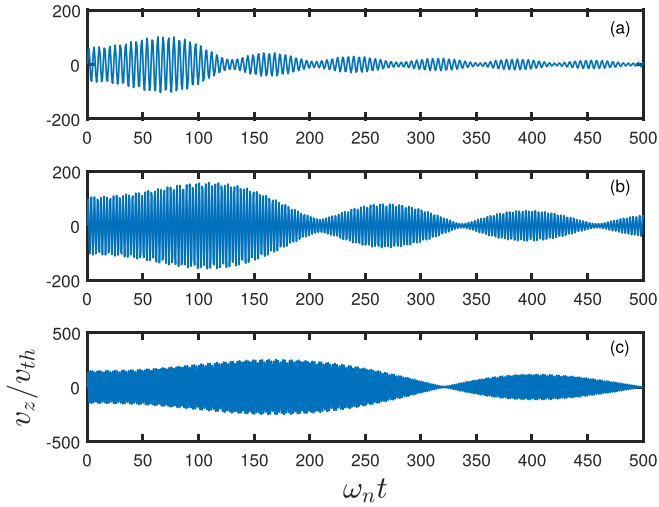
FIG. 2. Time evolution of $\hat{z}$ component of velocity v_z of a particle, initially located at the center of the monolayer and displaced vertically, is shown for three different cases with the changing values of ω_v. Here, for these three cases, the values of ω_v are chosen to be (a) $\omega_v = 1.3\omega_n$, (b) $\omega_v = 2.2\omega_n$, and (c) $\omega_v = 3.1\omega_n$. In these simulations, dust density and radius of initial perturbation are kept fixed at $n_d = 1.0n_0$ and $R = 5\lambda_D$, respectively.

information of the beat frequency. The Fourier spectra of v_z and v_{zm} are shown in Figs. 3(a) and 3(b), respectively, for three simulation runs with different values of ω_v. The Fourier spectra of $v_z(t)$ for the cases of $\omega_v = 1.3\omega_{pd}$ and $3.1\omega_{pd}$

are also shown in the zoomed scales in Figs. 3(c) and 3(d), respectively. From Figs. 3(a), 3(c), and 3(d), it is clearly seen that in all three cases, instead of a single peak (at $\omega = \omega_v$), Fourier spectra of $v_z(t)$ exhibit two distinctly separated peaks appearing as a sideband of the corresponding value of ω_v. However, the separation of these two peaks decreases (i.e., the sideband comes closer to the $\omega = \omega_v$) with the increase of ω_v. Figure 3(b) illustrates that in each case, a single peak representing the beat frequency appears in the Fourier spectra of $V_{zm}(t)$. It is also seen that the beat frequency decreases with the increase of ω_v and has the same value as the difference between two peaks (sideband) appearing in the corresponding Fourier spectra of $v_z(t)$. This indicates that a parametric decay instability occurs, which is responsible for the generation of sideband in the vertical oscillatory motions of the initially perturbed particles. Consequently, a train of pulses appears as a form of amplitude modulation initiated due to the interference of these sideband frequencies. The fundamental origin of this parametric process and its dependence on ω_v will also be discussed later in this section.

2. Dependence on dust density

We have also carried out simulations with changing values of dust density (n_d) in the 2D monolayer with a fixed confinement frequency $\omega_v = 1.3\omega_n$ and perturbation radius $R = 5\lambda_D$. In Figs. 4(a)–4(c), we have shown the time evolution of v_z of the tracked particle for three different values of n_d. Here also, we have seen that beats appear in the time profile of v_z. It has
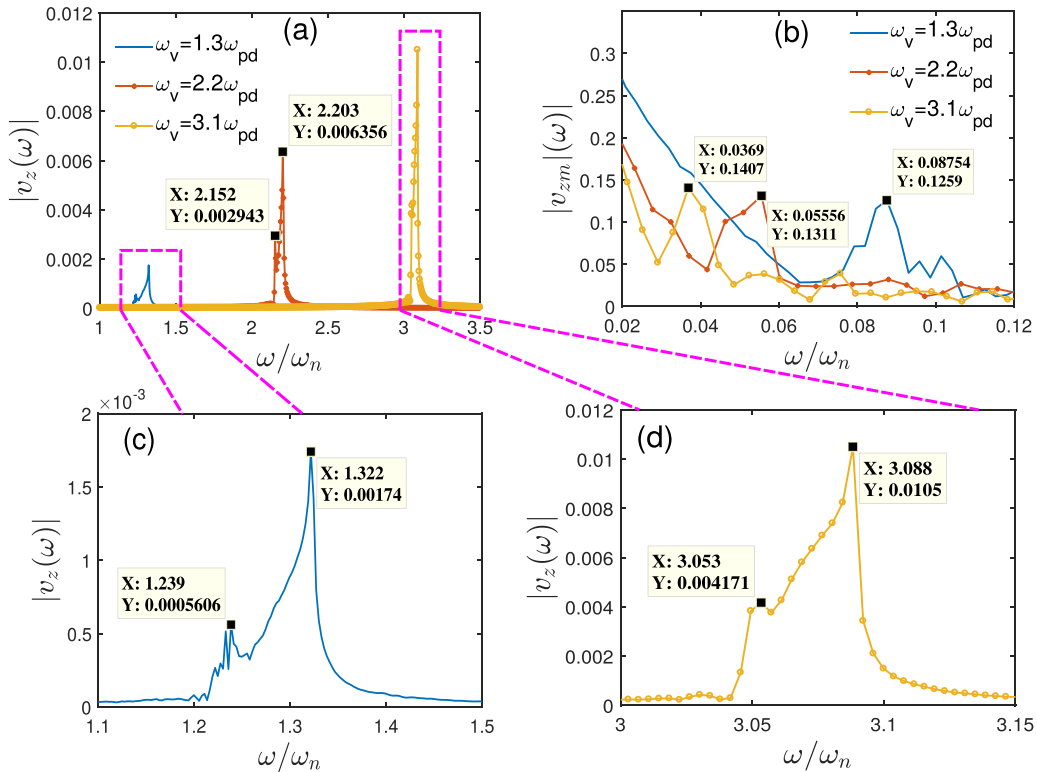

FIG. 3. Fourier spectra of $v_z(t)$ are shown in subplot (a) for three different cases with $\omega_v = 1.3\omega_n$, $2.2\omega_n$, and $3.1\omega_n$ with a fixed dust density $n_d = 1.0n_0$ and perturbation radius $R = 5\lambda_D$. The corresponding Fourier spectra of $v_{zm}(t)$ [peak values of $v_z(t)$] are illustrated in subplot (b). Fourier spectra of $v_z(t)$ for $\omega_v = 1.3\omega_n$, $3.1\omega_n$ are also depicted in the zoomed scales in subplot (c) and (d), respectively.
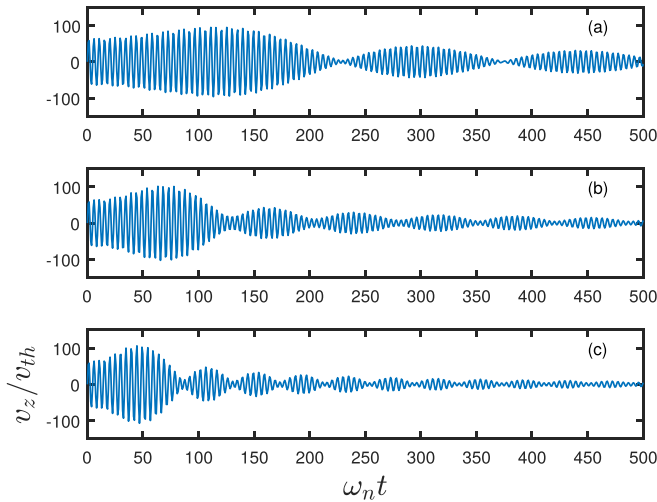
FIG. 4. The time series data of $v_z(t)$ of a particle initially located at the center of the monolayer are shown for three different cases with changing values of dust density (a) $n_d = 0.75n_0$, (b) $n_d = 1.0n_0$, and (c) $n_d = 1.25n_0$ with a fixed confinement potential frequency $\omega_v = 1.3\omega_n$ and perturbation radius $R = 5\lambda_D$.

been observed that the beat frequency and decay rate of the beat amplitude increase with an increase of n_d.

To capture the parametric process involved behind the formation of the beat in the vertical oscillatory motion of particles, we have evaluated Fourier spectra of $v_z(t)$ and $v_{zm}(t)$ as before for different values of n_d. From Fig. 5(a), it is seen that instead of a single peak at $\omega = \omega_v$, Fourier spectra of $v_z(t)$ in each case reveal broad spectra with two distinctly separated peaks. It is also seen that the separation between these two peaks increases with the increase of n_d. Fourier spectra of $v_{zm}(t)$ shown in Fig. 5(b) demonstrate that beat has a particular frequency which increases with the increase of n_d. Here also, it is seen that in each case, the beat frequency has the same value as the difference between two peaks that appeared in the corresponding Fourier spectra of $v_z(t)$. Thus, in these cases also, parametric decay instability is responsible for the generation of sidebands in the vertical oscillations of the particles.
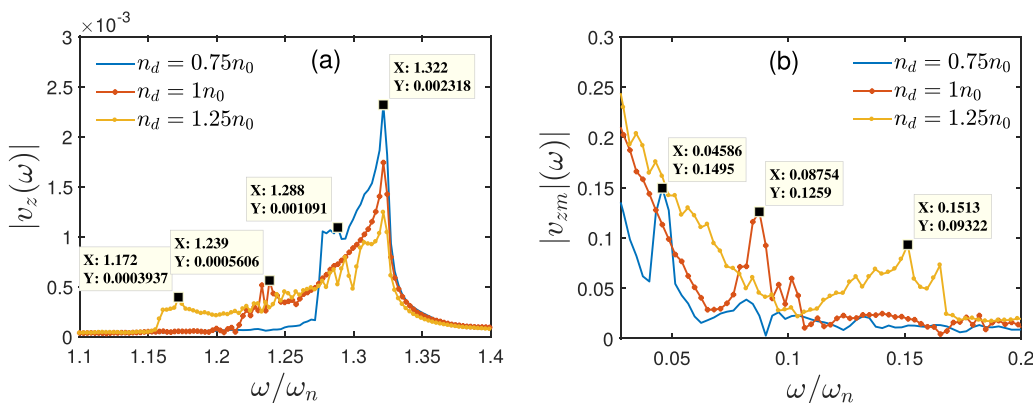
3. Dependence on perturbation radius

As mentioned earlier, the amplitude modulation phenomena initiate only when the initial perturbed region's size is less than that of the monolayer. When the entire monolayer is perturbed, the whole plane exhibits sinusoidal oscillation around the equilibrium height, i.e., $z = L_z/2$, without forming any beat or train of pulses in the particle's motion. However, to study the effect of the perturbation area, we have performed a few simulations with changing values of radius (R) of the initially perturbed region. The time evolution of $v_z(t)$ and the corresponding Fourier spectra of a tracked particle initially located at the center of the monolayer has been shown in Fig. 6 for three different values of R. It has been observed that the modulated amplitude becomes higher for higher values of R, as can be seen from Figs. 6(a)–6(c). It is also seen that for higher values of R, modulation occurs at a later time. This is a consequence of the fact that amplitude modulation initiates at the boundary of the perturbed and unperturbed regions. Thus, for higher values of R, it takes longer times to reach the information at the center of the monolayer where the chosen particle is located. However, the beat frequency does not change with the radius (R) of the perturbed region, as clearly depicted in Fig. 6(d).

The effect of initial displacement (d) on the properties of the medium has been reported in an earlier study where we have shown that crystalline monolayer melts through a first-order phase transition above a threshold value of d [9]. In that study, it has also been shown that this threshold value of d for which the phase transition occurs depends upon the value of R.

Let us now summarize all the results so far that have been presented and understand the fundamental origin behind the amplitude modulation phenomena observed in our study. As we impose an external perturbation by displacing a few particles initially located in the monolayer's central regime, they oscillate vertically under parabolic confinement potential. However, the dynamics of particles are strongly coupled with each other via pair interactions. As a result, a shear stress is generated between the neighboring particles, which triggers a nonlinear parametric process. Consequently, sidebands develop (Figs. 3 and 5) in the frequency spectra

FIG. 5. Fourier spectra obtained from the time series data of $v_z(t)$ and $v_{zm}(t)$ (peak values of v_z) for three different cases with changing values of 2D dust density $n_d = 0.75n_0$, $1.0n_0$, and $1.25n_0$ are shown in subplots (a) and (b), respectively. In these simulations, the confinement potential frequency and perturbation radius are fixed at $\omega_v = 1.3\omega_n$ and $R = 5\lambda_D$, respectively.
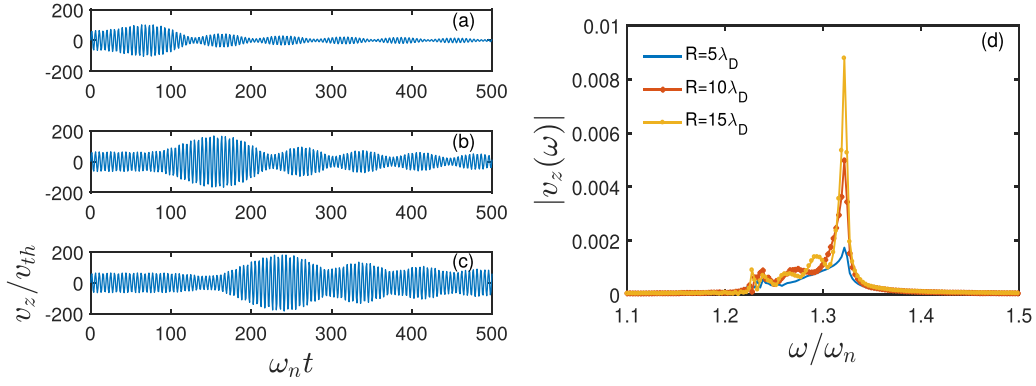
FIG. 6. Time evolution of $v_z(t)$ for three different simulation runs with (a) $R = 5\lambda_D$, (b) $R = 10\lambda_D$, and (c) $R = 15\lambda_D$. In subplot (d), the corresponding Fourier spectra of $v_z(t)$ have been shown. In these simulations, the confinement frequency and particle density are kept fixed at $\omega_v = 1.3\omega_n$ and $n_d = 1.0n_0$, respectively.

of vertical oscillatory motions of the particles. Therefore, amplitude modulation occurs, and beats are generated through the interference of these sidebands. It is important to note that beat is formed not only in the dynamics of perturbed particles but also in the initially undisturbed region of the crystalline plane, as will be discussed in Sec. III D. The beat amplitude erodes in time as the kinetic energy of the perturbed particles is transported and distributed in the whole crystalline plane. With the increase of parabolic confinement frequency (ω_v), the amplitude of the oscillating velocity (i.e., kinetic energy) of perturbed particles increases. This causes the effective interaction between the neighboring particles to be less efficient and reduces the shear stress. As a result, beat frequency and beat amplitude decay rate decrease with the increase of ω_v. This has been depicted in Fig. 7(a) and also can be seen from Figs. 2 and 3. However, the average interparticle separation decreases as we increase the particle density (n_d) in the 2D monolayer. As a result, effective pair interaction strength between neighboring particles increases. Consequently, the nonlinearity in the parametric process re-

sponsible for the amplitude modulation increases. Therefore, beat frequency and beat amplitude decay rate increases with n_d. This is clearly illustrated in Fig. 7(b) and also shown in Figs. 4 and 5.

B. Effect of dust-neutral collisions

To investigate the effect of dust-neutral collisions on the parametric process observed in our study, we have also performed Langevin dynamics simulations using the framework of LAMMPS [48]. In these simulations, we incorporated the frictional drag and random kicks into the dust grains by neutral gas atoms. In equilibrium, the net force acting on any ith particle at any time t can be expressed as

$$m_d \frac{d^2 \mathbf{r}_i}{dt^2} = -Q \sum_{j=1}^{N-1} \nabla U(r_{i,j}) - Q \nabla V_{\text{ext}} - \nu m_d \dot{\mathbf{r}}_i + \zeta_i(t), \quad (2)$$

where ν represents the dust-neutral collision frequency and $\zeta_i(t)$ is the random force exerted by the neutral atoms on the ith particle.

As before, we have introduced the perturbation in the system, i.e., crystalline monolayer, by displacing a few particles in the central regime of the monolayer along the vertical direction. We performed a series of simulations with changing values of dust-neutral collision frequency (ν). In these simulations, the amplitude of initial displacement (d), perturbation radius (R), dust density (n_d) in the 2D monolayer, and external confinement frequency (ω_v) are kept fixed at $d = 1.0\lambda_D$, $R = 5.0\lambda_D$, $n_d = 1.0n_0$, and $\omega_v = 2.2\omega_n$, respectively. In Figs. 8(a)–8(e), we have shown the time evolution of $v_z(t)$ and corresponding Fourier spectra of a tracked particle located at the center of the monolayer obtained from four different simulations with changing values of ν. In all cases, beats are generated in the oscillatory motion of the particle, and the beat amplitude decays in time. However, the decay rate of beat amplitude is higher for higher values of ν, as shown in Figs. 8(a)–8(d). This is expected as the presence of dust-neutral collisions provides an additional dissipation in the dynamics of the particles. The Fourier spectra of $v_z(t)$ of the tracked particle for different values of ν reveal that the sideband appears at the same locations for all the cases, as shown in Fig. 8(e). Thus, the beat frequency does not change
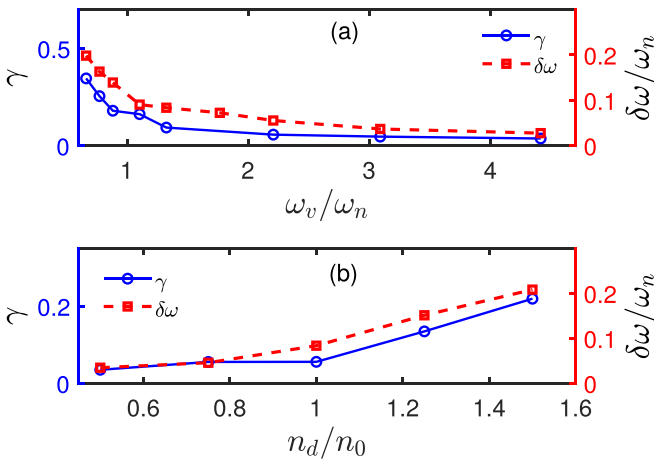

FIG. 7. The variation of beat amplitude decay rate (γ) and beat frequency ($\delta\omega$) as a function of (a) confinement frequency ω_v with a fixed $n_d = 1.0n_0$ and (b) particle density n_d in the 2D monolayer with a fixed $\omega_v = 1.3\omega_n$. The perturbation radius was kept fixed at $R = 5\lambda_D$ for all the cases.
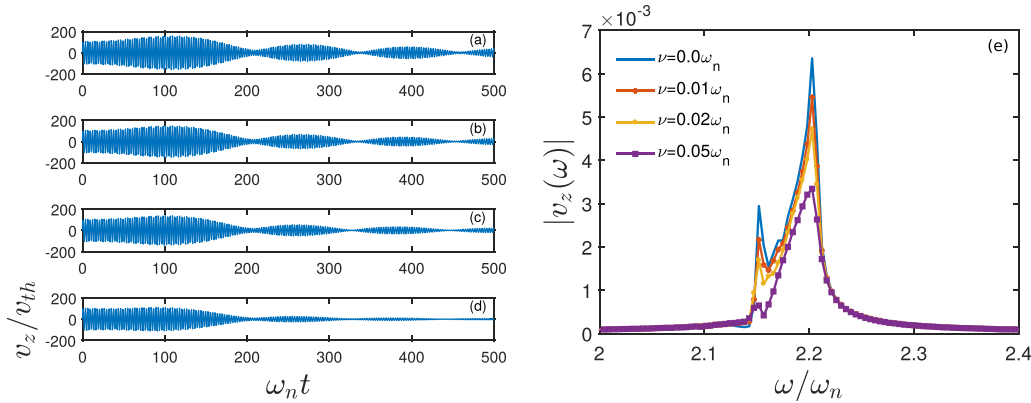
FIG. 8. Time evolution of $v_z(t)$ for four different simulation runs with dust-neutral collision frequency (a) $\nu = 0.0\omega_n$, (b) $\nu = 0.01\omega_n$, (c) $\nu = 0.02\omega_n$, and (d) $\nu = 0.05\omega_n$. In subplot (e), the corresponding Fourier spectra of $v_z(t)$ have been shown. In these simulations, the confinement frequency, particle density, and radius of perturbation are kept fixed at $\omega_v = 2.2\omega_n$, $n_d = 1.0n_0$, and $R = 5\lambda_D$, respectively. The initial perturbation amplitude (vertical displacement) is chosen to be $d = 1.0\lambda_D$ for all the cases.

with ν. This signifies that dust-neutral collisions do not affect the physical mechanism associated with the parametric decay process observed in our study. However, for very high values of dust-neutral collisions, the strength of the parametric process decreases. Thus, for higher values of ν, the energy associated with the initial perturbation (i.e., d and R) should be increased to excite the beat waves efficiently.

C. Theoretical model

We have also developed a simple theoretical model based on the arguments given above, which support our observations qualitatively. In our model, we have considered two particles coupled with each other via Yukawa pair interaction in the presence of an external parabolic potential [$V_{\text{ext}}(z)$]. One particle (particle 1) is subjected to an initial displacement in the vertical direction by a distance $z_1(t = 0) = -\lambda_D$ as in the case of MD simulations. The other particle (particle 2) is kept unperturbed initially. Thus, our model approximately mimics the boundary between perturbed and unperturbed regions of the monolayer. The schematic of the model is depicted in
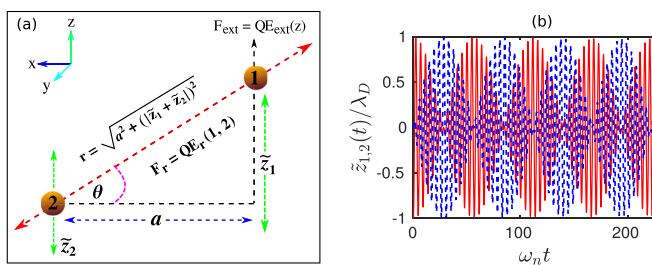
Fig. 9(a). The equations of motion of these two particles along the vertical ($\hat{z}$) direction can be expressed as

$$m_d \frac{d^2\tilde{z}_1}{dt^2} = -m_d\omega_v^2\tilde{z}_1 - \frac{Q^2}{4\pi\epsilon_0}\left[\frac{1}{r^2} + \frac{1}{r\lambda_D}\right]\exp\left(-r/\lambda_D\right)\sin\theta,$$
(3)

$$m_d \frac{d^2\tilde{z}_2}{dt^2} = -m_d\omega_v^2\tilde{z}_2 - \frac{Q^2}{4\pi\epsilon_0}\left[\frac{1}{r^2} + \frac{1}{r\lambda_D}\right]\exp\left(-r/\lambda_D\right)\sin\theta,$$
(4)

where $\sin\theta = (\tilde{z}_1 + \tilde{z}_2)/r$ with $r = \sqrt{a^2 + (|\tilde{z}_1^2 + \tilde{z}_2^2|)}$ representing the radial distance between the two particles. The first terms of the right-hand side (RHS) of Eqs. (3) and (4) represent the force $\mathbf{F}_{\text{ext}}$ associated with the external parabolic potential, $V_{\text{ext}}(z) = (m_d\omega_v^2/2Q)z^2$. The second terms of the RHS of these two equations represent the $\hat{z}$-component of the force $\mathbf{F}_r$ associated with Yukawa pair interaction between particles. We have solved Eqs. (3) and (4) numerically and shown the time evolution of $\tilde{z}_1$ and $\tilde{z}_2$ in Fig. 9(b). As in the case of MD simulations, it is seen that beat is formed in the time evolution of both perturbed and unperturbed particles. We also did a parametric study using our theoretical model, and the results are shown in Fig. 10. It is seen that beat frequency decreases with the increase of ω_v, as shown in Figs. 10(a)–10(c). Whereas, beat frequency increases with an increase of n_d, as have been shown in Figs. 10(d)–10(f). Here, the dependence of n_d is revealed through the parameter $a = \sqrt{1/\pi n_d}$ representing the average interparticle distance in the 2D crystalline plane. Thus, our simulation findings qualitatively agree with the numerical results obtained from the theoretical model. However, our theoretical model does not explain the damping of wave amplitude with time observed in our simulations. This is because of the fact that we have considered the dynamics of only two particles in our model, where the imparted energy always remains preserved within the dynamics of these two particles. In simulations, damping occurs because the external perturbation was introduced only within a small region of the crystal, and with time, the imparted perturbed energy transmits to the whole crystalline plane.

FIG. 9. A schematic of the theoretical model has been shown in subplot (a). In subplot (b), the time evolution of z coordinates of particle 1 ($\tilde{z}_1$) and particle 2 ($\tilde{z}_2$) obtained from the theoretical model have been shown by the blue dashed line and red solid line, respectively. Here, we have considered $\omega_v = 1.3\omega_n$ and $n_d = 1.0n_0$.
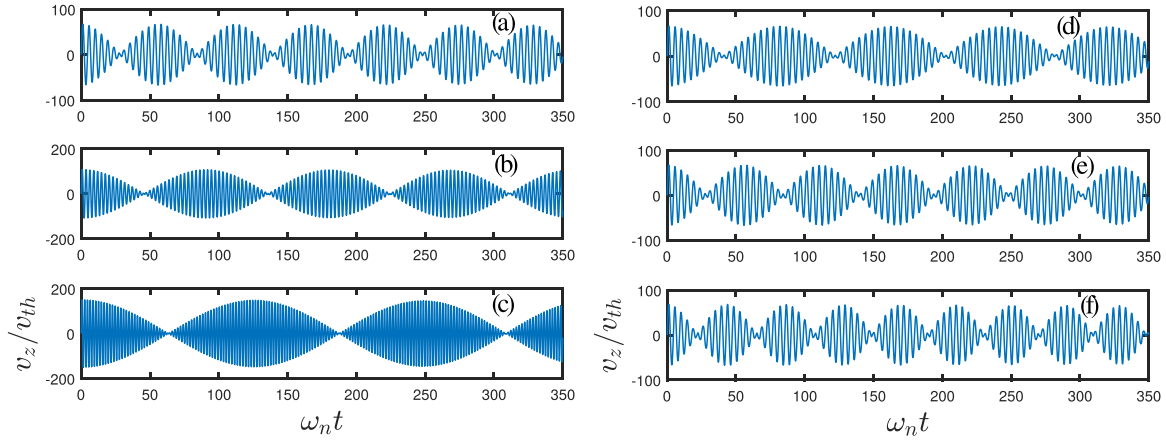
FIG. 10. Time evolution of $v_z(t)$ of a particle obtained from the theoretical model for three different values of confinement frequency, (a) $\omega_v = 1.3\omega_n$, (b) $2.2\omega_n$, and (c) $3.1\omega_n$ with a fixed $n_d = 1.0n_0$ have been shown. The same has been illustrated for three different values of dust density in subplots (d) $n_d = 0.75n_0$, (e) $n_d = 1.0n_0$, and (f) $n_d = 1.25n_0$ with a fixed $\omega_v = 1.3\omega_n$.

D. Surface wave generation

It would be interesting to look at how the rest of the monolayer, which was initially unperturbed, responds to the external disturbance imposed in the medium. The distributions of v_z in the x-y plane of the monolayer have been shown in Fig. 11 for different values of ω_v and n_d at a particular instant of time $\omega_n t = 900$. It is seen that in all the cases, the medium responds collectively to the initial external perturbation. It is seen that concentric circular wavefronts are generated in the profile of v_z around the initially perturbed region and spread over in the x-y plane of the crystalline layer. Moreover, at a particular instant of time, the area over which these circular wavefronts have been spread in the monolayer depends upon the values of ω_v and n_d, as can be seen from Figs. 11(a)–11(f).
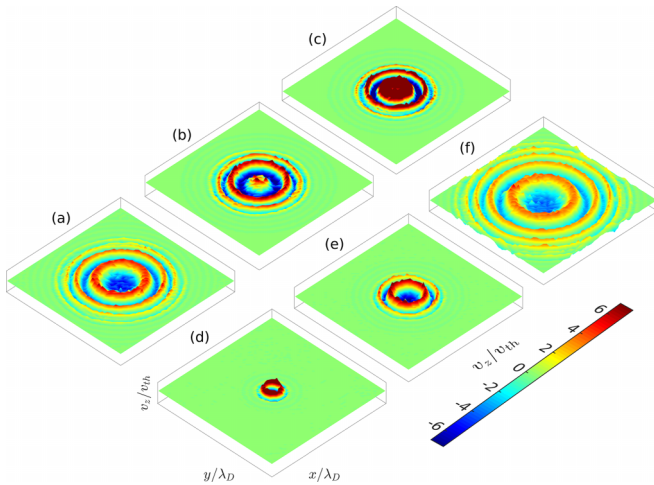

FIG. 11. Distributions of v_z in the xy plane of the monolayer is shown at a particular instant of time $\omega_n t = 900$ for different cases with the changing values of ω_v and n_d. In subplots (a)–(c) the values of ω_v are chosen to be $\omega_v = 1.3\omega_n$, $1.8\omega_n$, and $2.2\omega_n$, respectively for a fixed value value of $n_d = 1.0n_0$. In subplots (d) and (e), ω_v is kept constant at $\omega_v = 1.3\omega_n$ with the changing values of dust density $n_d = 0.5n_0$, $0.75n_0$, and $1.15n_0$, respectively. The perturbation radius is kept fixed at $R = 5\lambda_D$ for all the cases.

This is the consequence of the fact that the surface wave is generated through the formation of beat and beat frequency changes for different values ω_v and n_d.

It would also be interesting to see the particle-level dynamics while these circular waves propagate through the crystalline plane of the medium. For this purpose, we choose to track a particle initially located at a radial distance $r = 30\lambda_D$ from the center of the monolayer. It is to be noted that in this case, the radius of the initially perturbed region is to be $R = 5\lambda_D$. Thus, our chosen particle is located far away from the initial perturbation region. The dynamics of this tracked particle have been illustrated in Fig. 12. Time evolution of v_z of the tracked particle reveals the formation of beat, as depicted in Fig. 12(a). Thus, the beat occurs not only in the dynamics of initially perturbed particles but also for particles located in the initially undisturbed region of the monolayer. This has also been predicted from our theoretical model. It is also seen from Fig. 12(a) that the beat appears only after a certain time, which is the time the first wavefront takes to reach the location of the tracked particle. The Fourier spectra of $v_z(t)$, shown in Fig. 12(b), reveal that the vertical motion of the tracked particle is associated with two different frequencies. It is also seen that the difference between these two frequencies representing the beat frequency is the same as the perturbed particles, as shown in Fig. 3(b). Thus, the circular wavefronts propagating through the surface of the monolayer are nothing but the beat waves that originated due to the amplitude modulation of initial perturbation. The dynamics of the tracked particle in the x-z plane are demonstrated in Fig. 12(c) over the duration of a beat period. The position of the particle in the x-z plane at different times has been represented by the blue to red color symbols. It is seen that the particle exhibits oscillatory motion in the x-z plane. However, the mean position of the particle over a beat period almost remains unchanged. This reveals that the particle's motion has both transverse and longitudinal components, which is a typical characteristic of a surface wave.

The dispersion property of the surface wave observed in our study has been depicted in Fig. 13 in the ω-k plane. The dispersion relation has been obtained by measuring the wavelength and frequency (beat frequency, $\delta\omega$) of the fully
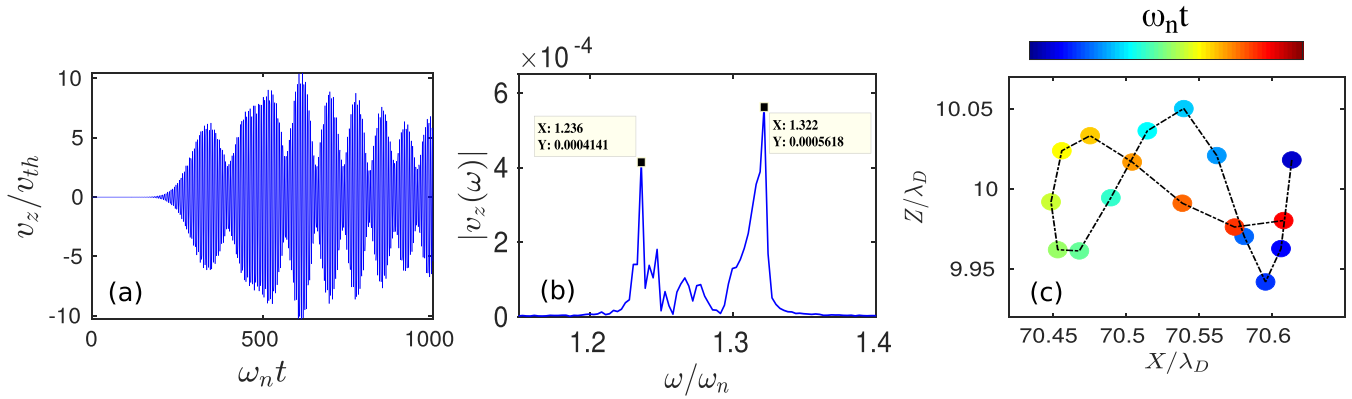
FIG. 12. Time evolution of v_z of a tracked particle located far away from the initially perturbed region ($R = 5\lambda_D$), i.e., $(x, y) = ((x_c - 30\lambda_D), y_c)$ is shown in subplot (a). Here, (x_c, y_c) represents the x-y coordinate of the center of the monolayer. In subplot (b), the Fourier spectra of $v_z(t)$ is depicted. The trajectory of the tracked particle in the $x - z$ plane in a chosen period of time is illustrated in subplot (c). Here, the color symbols from blue to red represent the evolution of time. In this simulation, we have considered $n_d = 1.0n_0$ and $\omega_v = 1.3\omega_n$.

developed surface waves with changing values of system parameters, i.e., ω_v and n_d. In both cases, we have obtained a linear dispersion relation between frequency ω and wave number k, as shown by the blue squares marked line and red circles marked line in Fig. 13, respectively. It is also seen that the dispersion relation obtained from our simulations closely matches the theoretical dispersion curve of the transverse shear wave shown by the solid black line in Fig. 13. The theoretical dispersion relation of the transverse shear wave has been obtained from the relation, $\omega \approx c_s k$, where $c_s = \sqrt{(k_B T/m_d)\Gamma} \exp{-(a/2\lambda_D)}$ is the velocity of the shear wave. Here, $\Gamma = Q^2/4\pi\epsilon_0 a k_B T$ represents the Coulomb coupling parameter. The measured group velocity of the surface wave observed in our simulation is $c_{\text{sim}} \sim 5.1$ mm/s, which is close to the theoretically estimated shear wave velocity, $c_s \sim 5.3$ mm/s. Thus, the surface waves observed in our study are the out-of-plane transverse shear waves generated due

to the velocity shear stress between neighboring particles. In our study, we have not considered the effect of ion flow in the vertical direction typically present in a dusty plasma experiment. The nonreciprocal interactions between particles at different heights originating from the ion wakes affect the transverse motions of the particles and, consequently, may alter the dispersion property of the observed surface wave. However, there were also experimental reports in the context of complex plasma systems where the effect of ion flow is insignificant [52,53].

IV. SUMMARY

In this study, we have investigated the response of a monolayer plasma crystal to an external perturbation under various conditions. We have performed 3D molecular dynamics simulations of a system of charged microparticles (dust) interacting via Yukawa pair interactions. In our simulations, we have also considered an external parabolic potential along the vertical ($\hat{z}$) direction, which mimics the combined effect of gravity and sheath electric field typically present in a dusty plasma experiment. It has been shown that a 2D monolayer of charged dust particles can be formed for a suitable choice of parabolic confinement frequency (ω_v) and dust density (n_d). We then imposed an external perturbation in the medium by displacing a few particles within a small circular region around the center of the monolayer along the vertical ($\hat{z}$) direction. We have analyzed in detail the response of the medium to this externally imposed perturbation under various conditions, e.g., changing values of ω_v, n_d, and R. It has been shown that the induced vertical oscillatory motion of the perturbed particles gets modulated through a parametric decay process initiated due to the shear stress between neighboring particles. Consequently, beat generates in the dynamics of both perturbed and initially unperturbed particles. As a result, concentric circular wavefronts are created, which propagate through the surface of the monolayer in the radially outward direction from the initially perturbed region. We have shown that these surface waves follow the dispersion relation of a transverse shear wave. The effect of dust-neutral collisions on the parametric
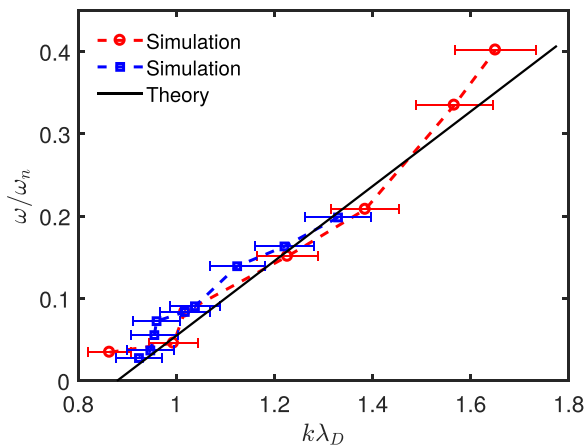

FIG. 13. Dispersion relation of the transverse surface wave in ω-k plane. The dispersion properties obtained by changing the values of n_d with a fixed $\omega_v = 1.3\omega_n$ are shown by the red circle-marked dashed line. The dispersion relation illustrated by a blue square-marked dashed line is for the case where we change the values of ω_v with a fixed dust density $n_d = 1.0n_0$.

process responsible for generating surface waves has also been demonstrated. A simple theoretical model has been provided supporting our simulation observations. An experimental realization of our simulation findings would be interesting. The effect of ion wakes on the phenomena observed in our study would also be an interesting aspect for future research.

The data cannot be made publicly available upon publication because they are not available in a format that is sufficiently accessible or reusable by other researchers. The data that support the findings of this study are available upon reasonable request from the authors.

[1] R. L. Merlino, J. Plasma Phys. **80**, 773 (2014).

[2] G. Morfill and H. Kersten, New J. Phys. **5**, 001 (2003).

[3] H. Thomas, G. E. Morfill, V. Demmel, J. Goree, B. Feuerbacher, and D. Möhlmann, Phys. Rev. Lett. **73**, 652 (1994).

[4] J. H. Chu and L. I, Phys. Rev. Lett. **72**, 4009 (1994).

[5] Y. Hayashi and K. Tachibana, Jpn. J. Appl. Phys. **33**, L804 (1994).

[6] S. Arumugam, P. Bandyopadhyay, S. Singh, M. Hariprasad, D. Rathod, G. Arora, and A. Sen, Plasma Sources Sci. Technol. **30**, 085003 (2021).

[7] V. A. Schweigert, I. V. Schweigert, A. Melzer, A. Homann, and A. Piel, Phys. Rev. Lett. **80**, 5345 (1998).

[8] S. Maity and A. Das, Phys. Plasmas **26**, 023703 (2019).

[9] S. Maity and G. Arora, Sci. Rep. **12**, 20430 (2022).

[10] A. Melzer, B. Buttenschön, T. Miksch, M. Passvogel, D. Block, O. Arp, and A. Piel, Plasma Phys. Controlled Fusion **52**, 124028 (2010).

[11] S. Maity, P. Deshwal, M. Yadav, and A. Das, Phys. Rev. E **102**, 023213 (2020).

[12] P. Deshwal, M. Yadav, C. Prasad, S. Sridev, Y. Ahuja, S. Maity, and A. Das, Chaos **32**, 063136 (2022).

[13] S. Maity, A. Das, S. Kumar, and S. K. Tiwari, Phys. Plasmas **25**, 043705 (2018).

[14] C. Killer, T. Bockwoldt, S. Schütt, M. Himpel, A. Melzer, and A. Piel, Phys. Rev. Lett. **116**, 115002 (2016).

[15] G. Arora, P. Bandyopadhyay, M. G. Hariprasad, and A. Sen, Phys. Plasmas **26**, 023701 (2019).

[16] G. Arora, P. Bandyopadhyay, M. G. Hariprasad, and A. Sen, Phys. Plasmas **26**, 093701 (2019).

[17] G. Arora, P. Bandyopadhyay, M. G. Hariprasad, and A. Sen, Phys. Plasmas **25**, 083711 (2018).

[18] G. Arora, P. Bandyopadhyay, M. G. Hariprasad, and A. Sen, Phys. Rev. E **103**, 013201 (2021).

[19] G. E. Morfill and A. V. Ivlev, Rev. Mod. Phys. **81**, 1353 (2009).

[20] P. Kaw and A. Sen, Phys. Plasmas **5**, 3552 (1998).

[21] S. Kumar, S. K. Tiwari, and A. Das, Phys. Plasmas **24**, 033711 (2017).

[22] G. Arora, P. Bandyopadhyay, M. G. Hariprasad, and A. Sen, Phys. Plasmas **27**, 083703 (2020).

[23] P. Shukla and A. Mamun, New J. Phys. **5**, 17 (2003).

[24] Y. Bailung, T. Deka, A. Boruah, S. Sharma, A. Pal, J. Chutia, and H. Bailung, Phys. Plasmas **25**, 053705 (2018).

[25] D. Samsonov, J. Goree, Z. W. Ma, A. Bhattacharjee, H. M. Thomas, and G. E. Morfill, Phys. Rev. Lett. **83**, 3649 (1999).

[26] Y. Bailung, B. Chutia, T. Deka, A. Boruah, S. K. Sharma, S. Kumar, J. Chutia, Y. Nakamura, and H. Bailung, Phys. Plasmas **27**, 123702 (2020).

[27] N. Rao, P. Shukla, and M. Y. Yu, Planet. Space Sci. **38**, 543 (1990).

[28] A. Barkan, R. L. Merlino, and N. D'angelo, Phys. Plasmas **2**, 3563 (1995).

[29] J. Pramanik, G. Prasad, A. Sen, and P. K. Kaw, Phys. Rev. Lett. **88**, 175001 (2002).

[30] F. Melandsø, Phys. Plasmas **3**, 3890 (1996).

[31] J. B. Pieper and J. Goree, Phys. Rev. Lett. **77**, 3137 (1996).

[32] S. Nunomura, D. Samsonov, and J. Goree, Phys. Rev. Lett. **84**, 5141 (2000).

[33] S. V. Vladimirov, P. V. Shevchenko, and N. F. Cramer, Phys. Rev. E **56**, R74 (1997).

[34] B. Liu, K. Avinash, and J. Goree, Phys. Rev. Lett. **91**, 255003 (2003).

[35] S. Vladimirov, V. Yaroshenko, and G. Morfill, Phys. Plasmas **13**, 030703 (2006).

[36] I. Kourakis and P. K. Shukla, Phys. Plasmas **11**, 2322 (2004).

[37] B. Farokhi, M. Shahmansouri, and I. Kourakis, Phys. Plasmas **16**, 053706 (2009).

[38] K. Qiao and T. W. Hyde, Phys. Rev. E **68**, 046403 (2003).

[39] D. Samsonov, S. Zhdanov, and G. Morfill, Phys. Rev. E **71**, 026410 (2005).

[40] L. Couëdel, V. Nosenko, S. K. Zhdanov, A. V. Ivlev, H. M. Thomas, and G. E. Morfill, Phys. Rev. Lett. **103**, 215001 (2009).

[41] L. Couëdel and V. Nosenko, Phys. Rev. E **105**, 015210 (2022).

[42] S. Takamura, T. Misawa, N. Ohno, S. Nunomura, M. Sawai, K. Asano, and P. Kaw, Phys. Plasmas **8**, 1886 (2001).

[43] M. Amin, G. Morfill, and P. Shukla, Phys. Plasmas **5**, 2578 (1998).

[44] S. Nunomura, T. Misawa, N. Ohno, and S. Takamura, Phys. Rev. Lett. **83**, 1970 (1999).

[45] S. Weber and C. Riconda, High Power Laser Sci. Eng. **3**, e6 (2015).

[46] T. Oosako, Y. Takase, A. Ejiri, Y. Nagashima, Y. Adachi, H. Kasahara, T. Yamada, O. Watanabe, H. Tojo, S. Kainaga *et al.*, Nucl. Fusion **49**, 065020 (2009).

[47] S. Maity, L. P. Goswami, A. Vashistha, D. Mandal, and A. Das, Phys. Rev. E **105**, 055209 (2022).

[48] S. Plimpton, J. Comput. Phys. **117**, 1 (1995).

[49] S. Nosé, Mol. Phys. **52**, 255 (1984).

[50] S. Nosé, J. Chem. Phys. **81**, 511 (1984).

[51] W. G. Hoover, Phys. Rev. A **31**, 1695 (1985).

[52] M. Zuzic, A. V. Ivlev, J. Goree, G. E. Morfill, H. M. Thomas, H. Rothermel, U. Konopka, R. Sütterlin, and D. D. Goldbeck, Phys. Rev. Lett. **85**, 4064 (2000).

[53] P. Hartmann, Z. Donkó, G. J. Kalman, S. Kyrkos, K. I. Golden, and M. Rosenberg, Phys. Rev. Lett. **103**, 245002 (2009).